

# We are IntechOpen, the world's leading publisher of Open Access books Built by scientists, for scientists

**4,800**

Open access books available

**122,000**

International authors and editors

**135M**

Downloads

Our authors are among the

**154**

Countries delivered to

**TOP 1%**

most cited scientists

**12.2%**

Contributors from top 500 universities



**WEB OF SCIENCE™**

Selection of our books indexed in the Book Citation Index  
in Web of Science™ Core Collection (BKCI)

Interested in publishing with us?  
Contact [book.department@intechopen.com](mailto:book.department@intechopen.com)

Numbers displayed above are based on latest data collected.

For more information visit [www.intechopen.com](http://www.intechopen.com)



# Biomedical Applications of Biomaterials Functionalized with Magnetic Nanoparticles

*Matteo Bruno Lodi and Alessandro Fanti*

## Abstract

The combination of magnetic nanoparticles and a biocompatible material leads to the manufacturing of a multifunctional and remotely controlled platform useful for diverse biomedical issues. If a static magnetic field is applied, a magnetic scaffold behaves like an attraction platform for magnetic carriers of growth factors, thus being a potential tool to enhance magnetic drug delivery in regenerative medicine. To translate in practice this potential application, a careful and critical description of the physics and the influence parameter is required. This chapter covers the mathematical modeling of the process and assesses the problem of establishing the influence of the drug delivery system on tissue regeneration. On the other hand, if a time-varying magnetic field is applied, the magnetic nanoparticles would dissipate heat, which can be exploited to perform local hyperthermia treatment on residual cancer cells in the bone tissue. To perform the treatment planning, it is necessary to account for the modeling of the intrinsic nonlinear nature of the heat dissipation dynamic in magnetic prosthetic implants. In this work, numeric experiments to investigate the physiopathological features of the biological system, linked to the properties of the nanocomposite magnetic material, to assess its effectiveness as therapeutic agents are presented.

**Keywords:** biomaterials, bone tumors, bone repair, drug delivery, hyperthermia, magnetic nanoparticles, RF heating, scaffolds

## 1. Introduction

Nanotechnologies aim to ease and to satisfy the needs of regenerative medicine<sup>1</sup> by providing multifunctional, theranostic, and stimuli-responsive biomaterials [1, 2]. In particular, stimuli-responsive biomaterials such as magneto-responsive biomaterials are devices capable of reacting to an external magnetic field spatio-temporally in a specific way [3]. This powerful class of biomaterials is a promising candidate as active and therapeutic scaffolds for advanced drug delivery and tissue regeneration applications [3, 4].

Multifunctional magnetic-responsive materials can be manufactured by modifying or functionalizing traditional materials employed in tissue engineering or by

---

<sup>1</sup> Regenerative medicine is a tissue regeneration technique based on the replacement or repair of diseased tissue or organs to restore a lost or impaired function [1].

Type of scaffold	Synthesis technique	$M_s$ , $\text{emu}\cdot\text{g}^{-1}$	Type of MNPs	$r_{mnp}$
HA/collagen	Impregnation	0.35–15	$\text{Fe}_3\text{O}_4$	200
HA/collagen	Impregnation	0.50	$\gamma\text{-Fe}_2\text{O}_3$ , $\text{Fe}_3\text{O}_4$	10–50
HA/PLA	Electrospinning	0.05	$\gamma\text{-Fe}_2\text{O}_3$	5
$\beta$ -TCP	Impregnation	0.6–1.2	$\text{Fe}_3\text{O}_4$	250
Chitosan/PVA membrane	Electrospinning	0.7–3.2	$\text{Fe}_3\text{O}_4$	n.s.
Calcium silicate/chitosan	Mixture	6–10	$\text{SrFe}_{12}\text{O}_{19}$	500
PMMA	Mixture	n.s.	$\text{Fe}_3\text{O}_4$	10
Silicate	Mixture	n.s.	$\gamma\text{-Fe}_2\text{O}_3$	n.s.
Fe-doped HA	Chemical substitution	4	HA- $\text{Fe}_3\text{O}_4$	10–14
Fe-hardystonite	Chemical doping	0.1–1.2	$\text{Fe}_3\text{O}_4$	20–60
Bredigite	Milling	7–25	$\text{Ca}_7\text{MgSi}_4\text{O}_{16}\text{-Fe}_3\text{O}_4$	120
HA	Impregnation	12–20	$\text{Fe}_3\text{O}_4$	200
HA	Impregnation	1–2.5	$\gamma\text{-Fe}_2\text{O}_3$	8
HA	Impregnation	n.s.	$\gamma\text{-Fe}_2\text{O}_3$	5
Chitosan	In situ precipitation	4	$\gamma\text{-Fe}_2\text{O}_3$ , $\text{Fe}_3\text{O}_4$	n.s.
$\epsilon$ -PCL	3D Bioplotting	0.2–0.3	$\text{Fe}_3\text{O}_4$	25–30
PLGA	Electrospinning	2–10	$\text{Fe}_3\text{O}_4$	8.47

**Table 1.**

*Magnetic scaffolds divided by composition, production, and MNPs embedded. Redrafted from [5].*

incorporating magnetic nanoparticles (MNPs) in the biocompatible matrix [4, 5]. **Table 1** reports examples of several magnetic biomaterials synthesized in the literature [6]. An approach to create a magnetic biomaterial is the impregnation of a polymer or ceramic (e.g.,  $\epsilon$ -poly caprolactone or hydroxyapatite) with MNPs dispersed in a ferrofluid (FF) [5, 6]. Subject to the action of capillarity, the nanoparticles fill the superficial defects and pores of the biomaterials. In this way a nanocomposite is created, i.e., the final material is a two-phase system strengthened by the magnetic iron phase [7]. Moreover, a multifunctional and composite material of such type can be obtained by the polymerization of a polymer in the presence of magnetic nanoparticles of magnetite ( $\text{Fe}_3\text{O}_4$ ) or maghemite ( $\gamma\text{-Fe}_2\text{O}_3$ ). This allows to produce a solid object using rapid prototyping and additive manufacturing techniques, such as electrospinning or 3D bioplotting [7].

In alternative, a stable, repeatable, and controllable manufacturing technique of magnetic-responsive biomaterial is the chemical doping of or substitution with  $\text{F}^{2+}$  or  $\text{F}^{3+}$  ions in a ceramic material (e.g., hydroxyapatite,  $\beta$ -tricalcium phosphate, and hardystonite). This process gives rise to an intrinsic magnetic and biocompatible material, which can be used in the form of microparticles or directly as a bulk object with tunable and ad hoc properties for therapeutic or regenerative medicine applications [8, 9].

Given these methods, the magnetic biomaterial can be processed to develop a tissue-guiding structure or a tissue scaffold, i.e., a device intended to be implanted in an injured site for supporting and withstanding the cell adhesion, proliferation, and differentiation, in order to restore tissue continuity and functioning [10]. Magnetic scaffolds (MagS) have been proposed for the following three main applications, as presented in **Figure 1** [1–9]:

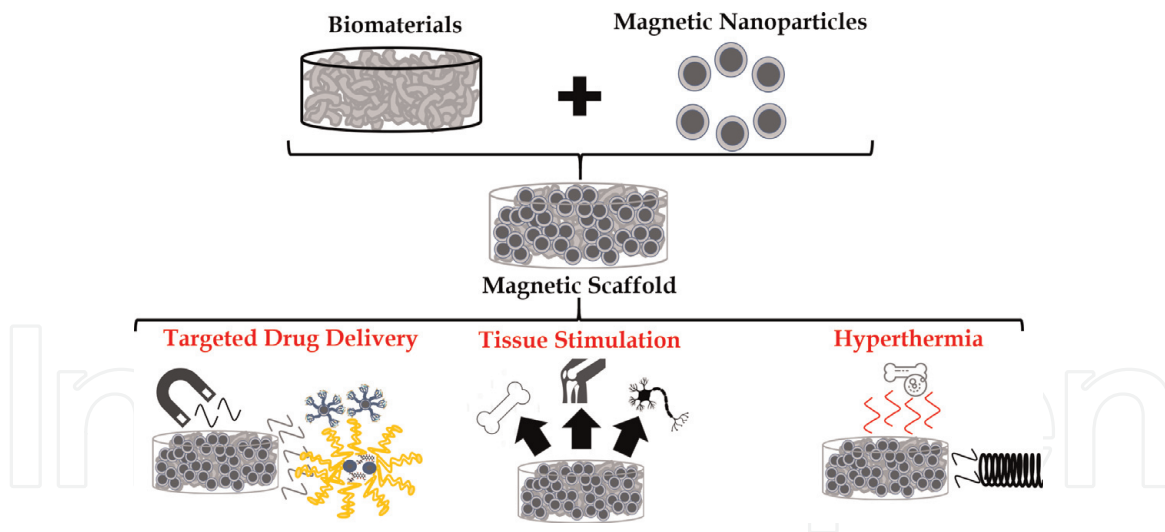


**Figure 1.**

Magnetic scaffolds are obtained by the combination of biomaterials and MNPs. They are multifunctional and theranostic nanocomposites. The potential biomedical applications of MagS are shown.

- To provide a controlled *mechanical stimulation* of tissues and boost the healing response
- To develop a smart and reliable *magnetic drug delivery system* (MDD)
- To generate therapeutic heat and perform local *hyperthermia* (HT) against cancer cells

The mechanical stimulation of injured tissues using magneto-responsive scaffolds found application in bone tissue engineering, where static magnetic field (SMF) or low-frequency magnetic field is used to elicit osteoprogenitor cells [1–4].

The rationale of employing magnetic scaffolds as part of a MDD system is the need to have an “attraction platform” to target and control the attraction of magnetic liposomes or MNPs bio-conjugated with growth factors (GFs) [6, 11]. Indeed, recently several magnetic carriers of biomolecules capable of acting on cell function were developed. However, using an external SMF their delivery to deep tissue and to the site of damage is complicated, and the MNPs tend to distribute where the magnetic force is maximum, i.e., at the body surface, where the field is applied [12]. Having a MagS implanted in the injured tissue allows to attract the MNPs and the GFs while controlling their spatial distribution [13].

Finally, if the external magnetic stimulus is a radio-frequency (RF) magnetic field, the population of MNPs embedded in the biomaterial dissipates a huge amount of heat. The deposited power can be exploited as therapeutic heat, enabling to use the magnetic scaffold as a thermo-seed able to perform HT treatment against cancer cells [14].

To date, magnetic scaffolds have been synthesized and characterized in terms of chemical and physical properties while proving experimentally their powerful and promising potential in regenerative medicine and oncology [1–4]. However, to translate the use of these nanostructured biomaterials in the clinical practice, several limitations have to be overcome, and further investigations are required to predict their behavior [4]. The potential use of magnetic scaffolds as tissue substitutes needs the combined work of material scientists, biomedical engineers, and biologists. In particular, since in the literature there is a clear lack of mathematical and numerical models, which relate the physical properties of these nanocomposite

biomaterials with the magnetic drug delivery or the hyperthermia, in this chapter, two mathematical models for their use as hyperthermia agent and as a tool for magnetic drug delivery are provided.

Section 2 briefly reviews the use of MagS as magneto-responsive biomaterials for the stimulation of tissues, in particular bone tissues. In Section 3 the nonlinear chemico-physical properties of magnetic scaffolds are presented, described, and used to introduce a recent *in silico* model for the planning of bone tumor hyperthermia [14]. Finally, in Section 4 the use of MagS as tool for active magnetic drug delivery is discussed. Furthermore, a mathematical model able of providing insights into the parameters of influence of the phenomenon is presented and analyzed [13]. The complete description of magnetic scaffolds favors the assessment of their effectiveness and their potential clinical impact.

## 2. Magnetic scaffolds for tissue repair and regeneration

Magnetic scaffolds have been tested both *in vitro* and *in vivo*, using animal models, demonstrating that they can transduce an external magnetic signal in mechanical stimulation to the cells attached to the biomaterial surface (**Figure 1**) [1–4]. MagS have been investigated for bone, cartilage, cardiovascular and neuronal regeneration, and repair [2]. The most studied tissue is bone. The injury of skeletal tissue by traumas and diseases, such as osteoporosis, or by a tumor resection calls for the need of a bone substitute or scaffold to guide cell adhesion, proliferation, and differentiation [15]. Moreover, the bone tissue requires a continuous mechanical stimulation. Therefore, the magneto-responsive biomaterials in **Table 1** can deliver a direct mechanical stimulation if exposed to SMF, to low-frequency magnetic field (strengths from to 18  $\mu\text{T}$  to 0.6 T, frequencies varying from 10 to 76.6 Hz), or to pulsed electromagnetic fields [4]. The mechanism of action is not fully understood yet. The presence of magnetic nanoparticles in the biomaterials determines an increased superficial roughness and favors the interaction at the cell membrane with the cell surface receptors. It has been demonstrated that the mesenchymal stem cells (MSCs) can differentiate into osteoblast thanks to the activation of the integrin signaling pathways, which upregulate the expression of the osteogenic GF bone morphogenetic protein 2 (BMP-2) [4]. The use of magnetic scaffolds permits the integration of the implant with the host tissue, accelerating the defect healing and increasing the mineral density of newly formed bone.

## 3. The hyperthermia treatment of bone tumors

### 3.1 The heat dissipation of magnetic nanoparticles

To understand the magnetization dynamic and the power losses of magnetic scaffolds, it is necessary to introduce the physical and mathematic descriptions of the response to a RF magnetic field of the MNPs embedded in it. If a population of magnetic nanoparticles in a solution is exposed to a harmonic RF magnetic field, they start to dissipate power due to the hysteresis loss but also to the magnetic dipole and to the Brownian relaxations [16]:

$$P_m = \pi\mu_0 f |\bar{H}|^2 \chi'' \quad (1)$$

where  $\mu_0$  is the vacuum permeability;  $f$  is the frequency of the applied field, in Hz;  $\bar{H}$  is the amplitude of the external magnetic field; and  $\chi''$  is the imaginary part of



the complex magnetic susceptibility of the particles. For ferrofluids, the magnetic susceptibility is known to be described by the Debye model [13, 16]:

$$\chi(f) = \chi' - j\chi'' = \frac{\chi_0}{1 + j2\pi f\tau} \quad (2)$$

The term  $\chi_0$  is the equilibrium susceptibility that is defined as [17]:

$$\chi_0 = \chi_i \frac{3}{\zeta} \left( \coth(\zeta) - \frac{1}{\zeta} \right) \quad (3)$$

where  $\zeta$  is the ratio between the magnetic energy of the set of magnetic dipoles and the thermal energy. Mathematically speaking:

$$\zeta(T) = \frac{\mu_0 \phi M_s^2 V_{mnp} |\bar{H}|}{3k_B T} \quad (4)$$

where  $M_s$  is the saturation magnetization of the single MNPs, in  $\text{Am}^{-1}$ ;  $V_{mnp}$  is the particle volume in  $\text{nm}^3$ ;  $k_B$  is the Boltzmann's constant; and  $T$  is system temperature. In Eq. (3),  $\chi_0$  is the initial susceptibility, which is defined as [17]:

$$\chi_i(\bar{H}, T) = \frac{\mu_0 \phi M_s V_m |\bar{H}|}{3k_B T} \quad (5)$$

The term  $\tau$  in the Debye model (Eq. 2) is the effective relaxation time, in s, which can be evaluated as the parallel of the Néel and Brownian processes [17]:

$$\frac{1}{\tau} = \frac{1}{\tau_N} + \frac{1}{\tau_B} \quad (6)$$

The time required to the magnetic dipole moment to align with the direction of the external magnetic field is called the Néel relaxation time,  $\tau_N$  [16, 17]:

$$\tau_N = \frac{\sqrt{\pi}}{2} \tau_0 \frac{e^\Gamma}{\Gamma} \quad (7)$$

The pre-exponential factor  $\tau_0$  is a time, and its value can range from 0.1 ps to 1 ns, but this term is a function of system temperature, i.e.,  $\tau_0 = \tau_0(T)$  [13]. The term  $\Gamma$  is the ratio of the anisotropy energy of the nanoparticle to the thermal energy of the system, i.e.:

$$\Gamma = \frac{K_a V_m}{k_B T} \quad (8)$$

where  $K_a$  is the magnetic anisotropy energy per unit volume in  $\text{Jm}^{-3}$  and  $V_m$  is the MNP volume in  $\text{nm}^3$ .

In a FF, the nanoparticles are allowed to rotate and move according to Brownian motion in the viscous medium where they are dispersed. When subject to a time-varying magnetic field, the particles rotate to orient with the direction of the external energy source, thus contributing to the relaxation process. The Brownian relaxation time can be evaluated as [16]:

$$\tau_B(\eta, T) = \frac{3\eta V_h}{k_B T} \quad (9)$$

being  $\eta$  the viscosity of the medium, in  $\text{Pa}\cdot\text{s}$ , and  $V_h$  the hydrodynamic radius of the particle in solution.

With Eqs. (1) to (9), it is possible to describe the frequency response and the power dissipation of a population of MNPs dispersed in a solution. This set of equations constitutes the theoretical basis for the understanding of magnetic scaffold behavior. However, since MagS are solid nanocomposites, the behavior of their magnetic phase is rather diverse than a FF. In the following, the experimental findings related to material characterizations and a new mathematical framework to account for their response are provided.

### 3.2 Hyperthermia response of magnetic scaffolds

Hyperthermia (HT) is a thermotherapy which aims at increasing the temperature of a target tissue between 41 and 46 C for about 60 min. For biological tissues, especially neoplasms and cancers, these temperatures are sufficient to damage the DNA of cells, altering its replication and also the repair pathways while determining cytotoxicity and activating the response of the host immune system [18, 19]. The rather chaotic vascular architecture of tumors is the reason of the thermo-sensibility of these pathologic tissues. The aforementioned biological effects can lead to the death of cancer cells, but, in the clinical practice, HT is exploited as a coadjuvant therapy combined with chemotherapy or/and radiotherapy rather than as a standalone therapy [19]. The hyperthermia can be induced using different types of energies, such as ultrasounds or electromagnetic (EM) field [14]. Currently different therapeutic modalities are available for HT induced by EM field. In particular, it is thoroughly investigated the local and in situ treatments using nanoparticles or magnetic scaffolds by exposing the target are with an external magnetic field.

Several magnetic scaffolds from **Table 1** demonstrated to be capable of noticeable temperature increases when exposed to magnetic field working at the frequencies from 100 kHz to 1 MHz and with amplitude ranging from 8 to 25 kAm<sup>-1</sup> [5, 7]. Different biomaterials (e.g., hydroxyapatite,  $\beta$ -TCP, and PCL) loaded with magnetite or maghemite nanoparticle temperature increase, from room temperature, of 8–45°C, were measured [5]. In particular, on one hand, a scaffold made with the intrinsic magnetic hydroxyapatite of Tampieri et al. [8] can increase the temperature of 40°C in 60 s when exposed to a magnetic flux density with amplitude of 30 mT and frequency 293 kHz. On the other hand, in the same exposure conditions, a PCL scaffold loaded with magnetite nanoparticles can raise the temperature from 20 to 32°C in 600 s [7, 8, 13].

These composite nanomaterials are identified as optimal candidates for local bone tumor hyperthermia [1–9, 13, 14]. However, their therapeutic potential must be investigated in a critique way. The understanding and the modeling of the heat dissipation of the MNPs embedded in the biomaterial are essential to allow an effective treatment planning.

### 3.3 The susceptibility spectra of magnetic scaffolds

The physical explanation of the relevant and significant temperature increases measured for MagS is not trivial. Moving from the theory explained in Section 3.1, the resonant Debye model cannot be applied to a system in which highly concentrated MNPs are fixed and embedded in a solid matrix and lattice or constrained in a highly viscous medium [13]. Indeed, the long-range interactions between the magnetic nanoparticles become relevant [20]. The following index  $\Upsilon$ , given in [20], can be considered to estimate the level of dipole–dipole interactions in the nanosystem under analysis:

$$\Upsilon = \frac{\mu_0 \mu_{mnp}^2}{4\pi k_B T d_{mnp}^3} \quad (10)$$

where the cubic power of the particle diameter,  $d_{mnp}^3$ , is the lower limit of the volume packaging and of the steric hindrance in the system [5]. For example, for magnetite nanoparticles the particle diameter measured in dry condition with transmission electron microscope (TEM) is lower than the hydrodynamic radius assessed using dynamic light scattering (DLS), i.e., 10 nm against 25 nm. Therefore, at the body temperature of 37°C, given the same dipole moment  $\mu_{mnp}$ , the level of interaction of MNPs in solution is 2.5 times lower. It is demonstrated by the morphological and structural characterization of MagS that the MNPs in the biomaterial are often aggregated or very near, implying that small clusters of nanoparticles can be identified [5]. Moreover, this last evidence supports the theory for which the relaxation dynamic of clusters of MNPs is strongly modified due to the appearance of a distribution of anisotropy energies [20]. In other words, the Néel relaxation time in Eq. (7) will depend on the number and the dispersion of sizes of the nanoparticles. Another limitation of the applicability of the Debye model to the description of magnetic scaffolds is the influence of Brownian relaxation time on the heat dissipation mechanism. It has been demonstrated that the frequency response of the complex magnetic susceptibility  $\chi(f)$  of MNPs modifies if the particles are constrained in agarose gel or used as cross-linkers in hydrogels [21, 22]. This change in the susceptibility spectra is due to the fact that in a highly viscous matrix or in a solid, the Brownian mechanism is hindered or canceled. From Eq. (9), in mathematical terms:

$$\lim_{\eta \rightarrow \infty} \tau_B(\eta, T) \rightarrow 0 \quad (11)$$

Therefore, in MagS the only relaxation time is the Néel one.

The influence of long-range interactions between particles, the modified distribution of anisotropy energy, and the different Néel relaxation dynamic are the factors that contribute to enhance the power dissipation of magnetic scaffolds, and all of them can help to explain the hyperthermia behavior of MagS, such as for the magnetic hydroxyapatite and the Fe-doped PCL scaffolds [7]. Relying on the magnetic susceptibility spectra of MNPs in agarose gel measured by Hergt et al. [21], a Cole-Cole model for magnetic scaffolds [13]:

$$\chi(\omega) = \frac{\chi_0}{1 + (2\pi f \tau)^{1-\alpha}} \quad (12)$$

Equation (12) can fit the susceptibility data, with a 1.5% relative error, as shown in **Figure 2**, whereas the Debye model cannot (Eq. (2)). In Eq. (12)  $\gamma$  is the broadening parameter, which is found to be equal to 0.75 [13]. The differences in the frequency response are depicted in **Figure 2**.

With Eqs. (1)–(8), but using Eq. (12) instead of Eq. (2), it is possible to evaluate and estimate the power losses of magnetic scaffolds. At this point it should be noted that the magnetic susceptibility  $\chi(f)$  is a function of the system temperature, which influences the initial susceptibility and the Néel relaxation time (Eqs. (5) and (7)). As the temperature increases, the therm  $\tau_0$  increases, whereas the time  $\tau_N$  decreases. The outcome is a decrease in the imaginary part of the magnetic susceptibility,  $\chi''$ , which in turn lowers the power deposited by the magnetic scaffold. Therefore, since the goal of hyperthermia treatment is to increase the temperature



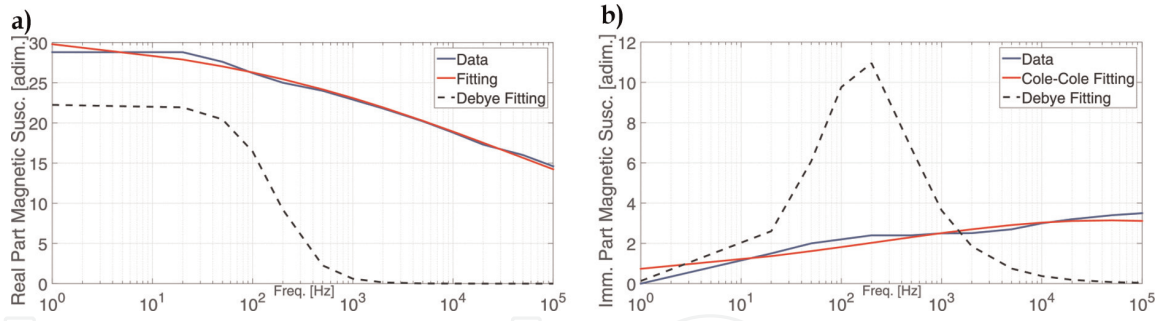


**Figure 2.** Results of the fitting of the magnetic susceptibility spectra of MNPs embedded in agarose: a) real part (in-phase) and b) imaginary (out-of-phase) components are presented [21]. The Debye and Cole-Cole models are used and compared Taken from [13].

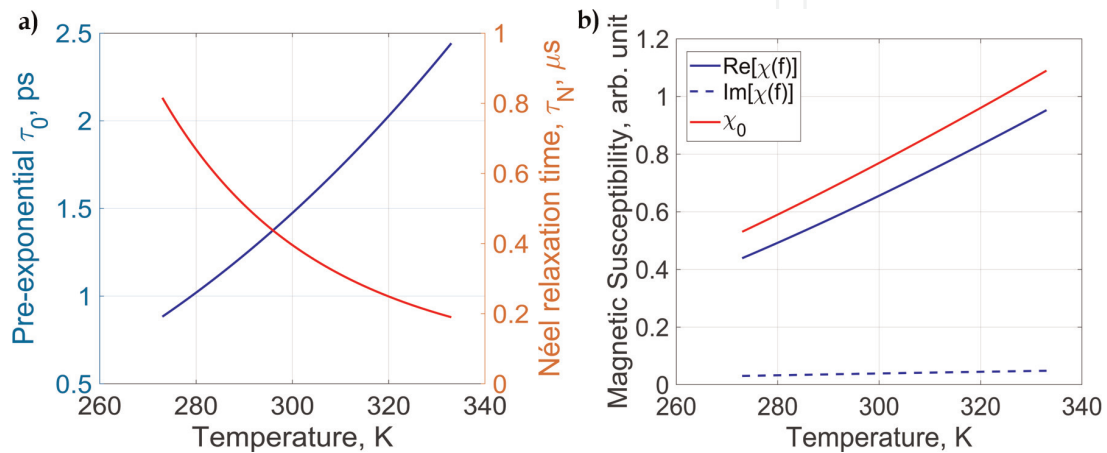


**Figure 3.** Temperature variation of the pre-exponential term  $\tau_0$  and the Neel relaxation time  $\tau_N$ . The influence on the equilibrium and the complex magnetic susceptibility  $\chi_0$  and  $\chi(f)$  is represented. The curves are obtained for a magnetic scaffold filled with the 0.2% of magnetite nanoparticles ( $r_{mnp}=10$  nm,  $M_s(0) = 2$  emu $\cdot$ g<sup>-1</sup>,  $T_b=150$  K).

of cancer tissues, it follows that the magnetic properties of and hence the power dissipated by MagS change during the treatment. The influence of temperature on the different physical quantities is shown in **Figure 3**. Since  $P=P(T)$ , planning a HT treatment which employs MagS as thermo-seeds against tumors is a multiphysics and highly nonlinear problem [14].

### 3.4 The hyperthermia treatment of bone tumors

Given the potential of magnetic scaffolds to be used as local heat source for setting the hyperthermia treatment of cancers, the most studied biological and clinical target of the nanosystems under investigation are bone cancers. Indeed, in clinical practice, currently available techniques such as chemotherapy, radiotherapy, and osteotomies presented a 15% probability of tumor recurrence, and therefore the hyperthermia treatment was proposed as adjuvant therapy [24]. Furthermore, since the surgical intervention causes a bone damage which calls for a graft or bone substitutes, magnetic scaffolds as theranostic, multifunctional, and magnetic-responsive biomaterials can be employed and can express their clinical potential [14].

Bone tumors are neoplasms mostly affecting subjects with age between 10 and 25 years old, causing impairment and pain, thus ruining the quality of life [23]. Malignant bone cancers such as osteosarcoma (OST) and fibrosarcomas (FIB) are known to affect long bone extremities [23]. OST and FIB are two different forms of bone cancer. The OST is big, aggressive and highly vascularized, whereas FIB is a poorly vascularized neoplasm. The survival rate for patients affected by OST and

FIB may vary from 28–40% [14, 23, 24]. To overcome these clinical issues, oncologist investigated the use of immunotherapy or smart nanocarriers of drugs, but local hyperthermia stands out as a very promising therapy [14]. The rationale is to implant a MagS after the bone tumor resection or reduction and then perform a local and in situ hyperthermia treatment by applying an external RF magnetic field. The residual cancer cells would be killed or increase their sensibility to drugs or radiations. Finally, the scaffolds would serve as supporting architecture for healthy cells, favoring tissue repair [14].

### 3.4.1 The *in silico* scenario

With the knowledge of the mechanism of power dissipation of MNPs embedded in a scaffold, recently a numerical scenario, with layered geometry, was proposed to investigate using finite element methods (FEM) the effectiveness of magnetic scaffolds in treating the residual bone cells of OST and FIB tumors [14].

As shown in **Figure 4**, imagining a surgical intervention of a bone cancer in distal femur, a spherical magnetic scaffold, with radius  $r_s = 5$  mm, is implanted to fulfill the bone cavity [14]. A small gap or fracture ( $r_f = 0.1$  mm) separates the scaffold from an annular region where the residual cancer cells of OST or FIB are supposed to be found. The fracture gap is a heterogeneous region where blood and bone are present, and it is where the new bone forms. It was demonstrated that its presence and biological status, i.e., if it is inflamed or ischemic, can influence the HT outcome [14]. The tumor area has a radius  $r_t$  which can vary from 0.1 to 0.5 mm. The goal of the HT treatment is to raise the temperature above 42°C for 30 min [14, 17]. Finally, a healthy bone tissue region with radius  $r_b = 5$  mm is included. The healthy bone should not be damaged by the treatment [5, 14]. It should be pointed out that muscle, fat, or skin tissues are not included in this analysis [25].

### 3.4.2 The electromagnetic problem

With respect to the geometry in **Figure 4**, the HT treatment using MagS is carried out applying an external RF magnetic field with strength  $H_0$ , working frequency  $f$  (293 kHz or 409 kHz [14]), and a time envelope able to keep the target temperature above the therapeutic threshold. The magnetic field is supposed to be

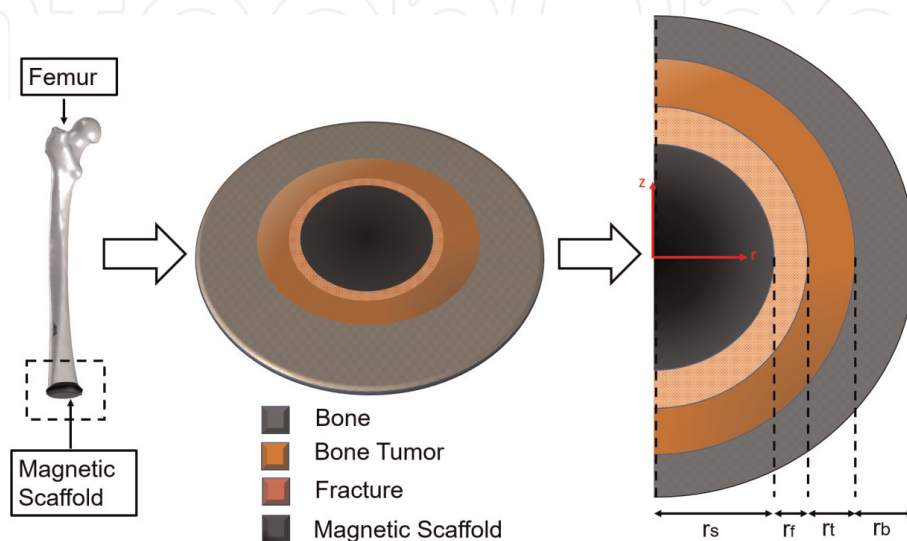


**Figure 4.** Simplified layered geometry for modeling the hyperthermia treatment of bone tumors using magnetic scaffolds. The MagS with radius  $r_s = 5$  mm is surrounded by a surgical fracture gap ( $r_f = 0.1$  mm), the area where residual cancer cells are present ( $r_t = 0.1$  mm–0.5 mm), and the healthy bone tissue ( $r_b = 5$  mm). Taken from [14].

homogeneous in space [14]. At the initial time, the system is supposed to be in thermal equilibrium with a constant temperature distribution ( $T_0=37^\circ\text{C}$ ). Maxwell's equation in the frequency domain should be solved to calculate the power dissipated in the system [5]:

$$\begin{aligned}\nabla \times \bar{H} &= j\omega(\epsilon_0\bar{E} + \bar{J}) \\ -\nabla \times \bar{E} &= -j\omega\mu_0\bar{H}\end{aligned}\quad (13)$$

where  $\omega$  is the angular frequency  $2\pi f$ ,  $\epsilon_0$  is the vacuum permittivity in  $\text{Fm}^{-1}$ ,  $\bar{E}$  is the electric field vector in  $\text{Vm}^{-1}$ , and, finally,  $\bar{J}$  conduction current vector in the system, in  $\text{A}\cdot\text{m}^{-2}$ . The total electromagnetic power dissipated is the sum of the power density dissipated by the scaffold and the tissues, i.e.,  $P_{EM} = P_m + P_e$ . The power deposited by the MagS,  $P_m$ , requires Eq. (13) to be solved considering the set of Eqs. (1)–(8) but using Eq. (12) instead of (2). The power dissipated by the induced currents in tissues ( $P_e$ ) cannot be neglected, even though several mathematical models related to magnetic hyperthermia did not include it [26]. However, the dielectric losses in the system can have a significant contribution to the final temperature increase while causing the unwanted indirect heating of the nontarget tissues [5, 25].

The EM problem is solved employing the *RF module* of the commercial FEM software COMSOL Multiphysics (COMSOL Inc., Burlington, MA). The MagS studied are the intrinsic magnetic hydroxyapatite and the PCL loaded with magnetite [7], as in [14]. The dielectric properties of scaffold and tissues at  $T_0$  are reported in **Table 2**.

### 3.4.3 The heat transfer problem

The power deposited by the MagS and conducted to the tissues in the system of **Figure 4** modifies the temperature ( $T = T(r, z, t)$ ), whose spatiotemporal evolution can be evaluated using the Pennes' bioheat equation [14]:

$$\rho C_p \frac{\partial T}{\partial t} = \nabla \cdot (k\nabla T) + \rho_b C_{p,b} \omega_b (T - T_a) + Q_{met} + P_{EM} \quad (14)$$

where  $\rho$  is the density in  $\text{g}\cdot\text{m}^{-3}$ ,  $C_p$  is the specific heat capacity in  $\text{Jkg}^{-1}\text{K}^{-1}$ , and  $k$  is the thermal conductivity in  $\text{Wm}^{-2}\text{K}^{-1}$ . The terms  $\rho_b$  and  $C_b$  are the density and heat capacity of blood, whereas the quantity  $\omega_b$  is the tissue perfusion, in  $\text{s}^{-1}$ , i.e., the capillary contribution which acts to equilibrate the tissues with the blood temperature  $T_b=37^\circ\text{C}$ .  $Q_M$  is the metabolic heat rate generated by the tissues, in  $\text{Wm}^{-3}$ .

Material or tissue	Re[ $\epsilon$ ]	$\sigma$ , $\text{Sm}^{-1}$
Magnetic hydroxyapatite	12.5	$2.1\cdot 10^{-3}$
$\epsilon$ -PCL	2.20	$10^{-4}$
Fracture gap–inflamed	3580	0.545
Fracture gap–ischemic	1321	0.196
Bone tumors: OST and FIB	8000	0.280
Bone	192	0.0214

**Table 2.**  
*Electromagnetic properties of scaffolds and tissues [14].*

Eq. (14) was implemented in COMSOL using the *Bio-Heat transfer module*. The initial temperature  $T_0$  was set in all domains. The bone edges are assumed to be open boundaries. The temperature field is continuous at each tissue interface. The thermal properties of materials and tissues employed are reported in **Table 3**.

The solution of Eq. (14) is a new temperature field. As previously discussed, the different system temperature determines a change in the magnetic and heat dissipation properties of the scaffolds. Also the dielectric and thermal properties of tissues vary with temperature [14]. To account for the influence of these variations on the outcome of HT treatment, the solution of Eq. (14) should be used to evaluate the EM power solving Eq. (13) for the next time step; then the next temperature distribution can be calculated considering the changed physical properties. This solution scheme is justified by the rather different dynamic of the EM and thermal fields [14].

In the temperature range 37°C–47°C of the HT treatment, the following linear relationship between the property  $p$  ( $\epsilon$ ,  $\sigma$ ,  $C_p$ ,  $k$ ) of each tissue and the system temperature [5, 14, 25]:

$$\frac{\Delta p(T)}{p(T_0)} = 1 + c\Delta T \quad (15)$$

The dielectric properties are assumed to increase linearly with  $c = 3\% \text{ C}^{-1}$  [14]. The thermal properties,  $C_p$  and  $k$ , have been assumed to vary with  $c = 0.5\% \text{ C}^{-1}$  and  $0.33\% \text{ C}^{-1}$ , respectively [14]. An exception was made for the heat capacity of blood, which presents a negative coefficient of  $-1\% \text{ C}^{-1}$  [14].

In this condition the strength, frequency, and envelope of the external RF magnetic field required to treat both osteosarcoma and fibrosarcoma cells were investigated.

### 3.5 Results

The temperature pattern resulting from the exposure to the homogeneous RF field is uniform and radial, as shown in **Figure 5a**. This is a consequence of the homogeneous distribution of the MNPs in the biomaterials [7, 14]. After 60 min of treatment, it can be noticed that the temperature in the healthy bone can reach 47°C, which is a potentially harming value. To assess the performance of the two types of MagS in treating OST and FIB, the average value of temperature in the tumor region vs. time was considered. From **Figure 5b** it can be noticed that both magnetic hydroxyapatite and Fe-doped PCL are able to treat the poorly vascularized FIS for any given dimension of the residual area  $r_t$ . This can be explained considering that  $P_{EM} \gg |\rho_b C_{p,b} \omega_b (T - T_a)|$ , for  $H_0 = 10\text{--}17 \text{ mT}$ . However,

Material or tissue	$k, \text{ W m}^{-1} \text{ K}^{-1}$	$C_p, \text{ J kg}^{-1} \text{ K}^{-1}$	$Q_m, \text{ W m}^{-3}$	$\omega_b, \text{ s}^{-1}$
Magnetic hydroxyapatite	1.33	700	—	—
e-PCL	0.488	3359.2	—	—
Fracture gap–inflamed	0.558	2450	5262.5	$6.95 \cdot 10^{-3}$
Fracture gap–ischemic	0.558	2450	5262.5	$6.95 \cdot 10^{-3}$
Bone tumors: OST and FIB	0.32	1313	57,240	$2.42 \cdot 10^{-3} \div 0.595$
Bone	0.32	1313	286.2	$0.262 \cdot 10^{-3}$

**Table 3.**  
 Heat transfer properties of scaffolds and tissues [14].



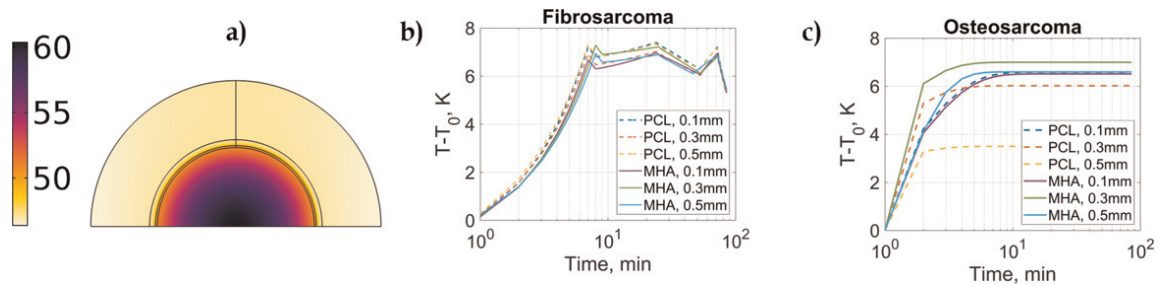


**Figure 5.**

(a) 2D temperature distribution after 60 min of treatment using a RF magnetic field of 30 mT and working at 293 kHz. A OST with  $r_t=0.5$  mm is considered. (b) Average temperature in the region with residual FIB cells. (c) Average temperature in the region with residual OST cells. (MHA = magnetic hydroxyapatite).

the temperature rise is noticeable, and the external field should be modulated (or turned off) to keep the temperature closest to the target value of 42°. In the case of OST, give the high value of blood perfusion (see **Table 3**); not all MagS are able to treat successfully the residual cancer cells. This is the most challenging tumor. Indeed, the Fe-doped PCL scaffold fails to reach the lethal HT temperature for an OST of 0.5 mm, even increasing the amplitude to 40 mT or the frequency to 409 kHz. The magnetic hydroxyapatite scaffold is more effective in treating the residual osteosarcoma cells, as can be observed in **Figure 5c**. These results demonstrate that the in HT treatment of residual bone tumor cells is feasible, and, with the knowledge of the physico-chemical properties of the nanomaterial, the treatment can be planned against different type of tumors.

## 4. Magnetic scaffolds and regenerative medicine

### 4.1 Magnetic drug delivery

Magnetic scaffolds were conceived as a multifunctional platform for tissue engineering applications (see **Figure 1**) [1–5]. As presented in the Introduction, they are a platform for magnetically targeted drug delivery of growth factors to control and enhance tissue healing, such as in the case of bone tissue [1, 11]. The bio-nanotechnology research developed magnetic carriers of biomolecules such as VEGF or TGF- $\beta$  [11, 27]; however, the problem of maximizing and controlling their delivery to the site of injury is still addressed in the literature [1–4, 13]. This section will cover the use of MagS, implanted in a damaged bone, as an in situ magnet, i.e., as attraction site for external MNPs carrying GFs. The influence on the cellular response is assessed employing a multiphysics model [13]. The prediction of the magnetic force required to attract the MNPs, the velocity in the extracellular matrix (ECM) medium, and the final spatial distribution is fundamental to foresee a treatment planning procedure, while evaluating the influence parameters in the drug delivery and the cellular migration process.

### 4.2 Challenging the mathematical modeling of MDD

#### 4.2.1 The magnetostatic problem

Considering the geometry of **Figure 4**, the analysis domain is limited to the scaffold and the fracture gap, neglecting the bone tumor and assuming that only healthy bone is present, in a way similar to [13]. The MagS and the gap have a radius



of 5 mm. An external uniform and static magnetic flux density field of strength  $B_0$  is supposed to be applied along the z-axis of the system. The magnetic composite nanomaterial will magnetize in a nonlinear way according to the following relationship [13]:

$$\bar{M} = M_s \phi \left( \coth(\zeta) - \frac{1}{\zeta} \right) \quad (16)$$

where all symbols have the previous definition. As presented in **Table 1**, the magnetization response of the scaffolds varies from a minimum of  $0.4 \text{ emu} \cdot \text{g}^{-1}$  to a maximum of  $25 \text{ emu} \cdot \text{g}^{-1}$ . Considering this nonlinear material property, the problem is the determination of the spatial distribution of the magnetic field, i.e., the solution of the following magnetostatic problem employing the scalar magnetic potential  $\psi_m$  [13]:

$$\begin{aligned} \nabla \times \bar{H} &= 0 \\ \bar{H} &= -\nabla \psi_m \end{aligned} \quad (17)$$

Due to the presence of the magnetic material, the magnetic field flux lines concentrate in the prosthetic implant, implying that the norm of the gradient of magnetic density field between the MagS and the diamagnetic tissues is relevant [6]. In the literature, it is reported that if the magnetic density field gradients are higher than  $1.3 \text{ Tm}^{-1}$ , then the magnetic force exerted on a population of surrounding MNPs would be sufficient to overcome their weight force and set them in motion toward the scaffold [13, 28]. This is a very simplified view of the problem. Indeed, several relevant physical and biological factors took part to the transport phenomena of MNP attraction to the MagS in the presence of a static magnetic field. As defined by Grief and Richardson, the magnetic force vector  $\bar{F}_m$  on an ensemble of MNPs in saturation regime can be evaluated as follows [12]:

$$\bar{F}_m = \frac{M_{s2} V_{m2}}{6k_B T} \nabla |\bar{B}|^2 \quad (18)$$

where  $M_{s2}$  and  $V_{m2}$  are the saturation magnetization, in  $\text{Am}^{-1}$ , and the volume of the spherical magnetic nanoparticles, in  $\text{nm}^{-3}$ , to be attracted, respectively. The nanoparticles conjugated with growth factors or drugs are hence set in motion with a velocity  $v_m$  equal to [12, 13]:

$$\bar{v}_m = \frac{\bar{F}_m}{6\pi\eta r_{m2}} \quad (19)$$

where  $r_{m2}$  is the radius of the magnetic carriers. The term  $\eta$  is the viscosity of the medium in which the nanoparticles move, in  $\text{Pa} \cdot \text{s}$ . This medium is often assumed to be water ( $\eta_w = 1 \cdot 10^{-3} \text{ Pa} \cdot \text{s}$ ); however, actually the MNPs that move from the capillaries of bone tissues into the fracture gap are dragged in a solution of water, proteins (e.g., collagen, fibrin, and plasmin), and other macromolecules. Therefore, the extracellular matrix (ECM) can be assumed to be the medium in which the MNPs move, implying that  $\eta_w = 1 \cdot 10^3 \text{ Pa} \cdot \text{s}$  [13].

After having solved Eq. (17) and calculated Eqs. (18) and (19), the spatiotemporal distribution of the concentration of MNPs ( $C_{mnp}$ ,  $\text{mol} \cdot \text{m}^{-3}$ ) functionalized with the drug can be obtained computing the following diffusion-convection equation [13]:

$$\frac{\partial C_{mnp}}{\partial t} = \nabla \cdot [D_{mnp} \nabla C_{mnp}] - \bar{v}_m \nabla C_{mnp} \quad (20)$$

$D_{mnp}$  is the diffusion coefficient of MNPs in the medium, assumed to be equal to  $10^{-9} \text{ms}^{-2}$ . The analytical mass balance is subject to the outflow condition at the scaffold surface, while a constant initial concentration of MNPs ( $C_{m,0}$ ) is assumed at the host bone interface. In the fracture gap, it is assumed that  $C_{mnp}(r, z, t = 0) = 0$  as initial condition.

The magnetic field distribution (Eq. (17)) is derived by solving numerically the magnetostatic problem for the geometry depicted in **Figure 4** using the *Magnetic Fields No Currents* package from the *AC/DC module* of COMSOL Multiphysics. Then  $\bar{v}_m$  is inserted in the *Transport of Dilute Species* interface to solve Eq. (20).

#### 4.2.2 Including the cells and the biological elements

Now, we assume that the MDD system is constituted by an active GF with concentration  $C_{chemo}$  present at the MNP surface. The presence of such specific biomolecule is supposed to represent a direct chemotactic stimulus for the human mesenchymal stem cells (MSCs) present in the surrounding host bone tissue [13]. Chemotaxis is the phenomenon of cellular migration directed toward a chemical stimulus. This means that the osteoprogenitor cells can respond to the chemical signaling stimulus carried by the MNPs. The magnitude of the chemotactic stimulus can be assumed to be equal to [13]:

$$K_{chemo} = \frac{D_c}{C_{chemo}} \quad (21)$$

Given  $C_{mnp}$  from Eq. (20), the spatial pattern of the MSCs exposed to the biological signal carried by the MNPs is the solution of the mass balance for the cell population  $C_c$ :

$$\frac{\partial C_c}{\partial t} = \nabla \cdot [D_c \nabla C_c - C_c K_{chemo} \nabla C_{mnp}] \quad (22)$$

Similar to Eq. (20), Eq. (22) is subject to Dirichlet and Neumann boundary conditions, i.e., the diffusive flux of cell population should be null at the scaffold surface, and the cell concentration at host bone is set to a constant value of  $C_{c,0}$ . Moreover, the cell concentration in the fracture gap is assumed to be null at the initial time.

With this set of equations, it is possible to model the role of magnetic scaffolds as part of a MDD system studying the influence on the cellular migration and the scaffold colonization, providing valuable insight into the use of MagS as a tool in tissue engineering.

#### 4.2.3 Results from the case study

The magnetic scaffolds exposed to the static magnetic flux density field  $B_0$  respond in a way similar to a uniformly magnetized sphere, as shown in **Figure 6a**. As a matter of fact, the magnetic force and resulting velocity distribution are similar, implying that the MNP concentration is maximum at the poles of the scaffold, while it is minimum at the equator (**Figure 6b**). The generic GFs attached to the MNPs are sensed by the cells, which migrate toward the chemical stimulus. As shown by **Figure 6**, after only 24 h of migration, the MSCs invade the gap cavity

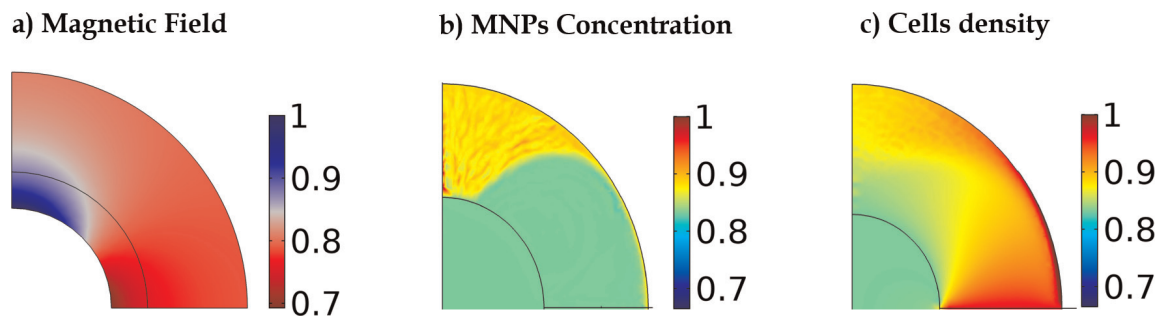


**Figure 6.** (a) Normalized magnetic field distribution ( $\bar{H}/H_0$ ). (b) Normalized MNP concentration profile after 48 h ( $C_{mnp}/C_{m,0}$ ). (c) MSC density after 24 h ( $C_c/C_{c,0}$ ).

and reach the biomaterial surface. This suggests that the cells can colonize the scaffold and boost the regenerative process. From the model and the results presented, the final cell density pattern can be predicted and controlled by tuning or acting on the scaffolds magnetic properties or geometry [13].

## 5. Conclusions

This chapter presented an innovative family of nanocomposite magnetic biomaterials and their biomedical applications. Mixing magnetic nanoparticles with traditional biomaterials, e.g., polymer or ceramics, or chemically doping them allows the manufacturing of a magnetic-responsive biomaterial with multifunctional properties. The so-called magnetic scaffolds have been studied for their ability to transduce an external magnetic signal into mechanical and biological outcome, thus proving to be a powerful platform for cell and tissue stimulation [1–4]. Exploiting the ability of the MNPs embedded in the biomaterial to dissipate power when exposed to a radio-frequency magnetic field makes MagS a valid candidate to perform local hyperthermia treatment on residual cancer cells. In this chapter the physical properties and the magnetic susceptibility of these novel composite nanosystems are investigated. Then an *in silico* model to study the feasibility of employing MagS in the treatment of bone cancers, such as osteosarcomas and fibrosarcomas, is presented [14]. The results indicate that further research on the nanomaterial is required to develop an effective and tailored magnetic scaffold. Finally, the potential of MagS to serve as an *in vivo* attraction site to enhance the magnetic drug delivery of growth factors is faced. To predict the final concentration pattern, a mathematical model which relates the nonlinear magnetic problem and the mass transport issue is presented. Furthermore, the link between these two aspects and the biological influence on cellular migration is challenged [13]. The results indicate that MagS are able to attract MNPs and exert an indirect action on MSCs in a way dependent on the geometrical and material properties.

## Acknowledgements

The authors would like to sincerely thank Prof. G. Mazzarella for the helpful discussions and suggestions to this work.

## Conflict of interest

The authors declare no conflict of interest.

## Abbreviations


BMP-2	bone morphogenetic protein-2
DLS	dynamic light scattering
ECM	extracellular matrix
FIB	fibrosarcoma
FEM	finite element method
FF	ferrofluid
GF	growth factor
MagS	magnetic scaffold
MDD	magnetic drug delivery
MF	magnetic field
MHA	magnetic hydroxyapatite
MSC	mesenchymal stem cell
MNP	magnetic nanoparticle
OST	osteosarcoma
PCL	poly-caprolactone
RF	radio frequency
SMF	static magnetic field
TCP	tricalcium phosphate
TEM	transmission electron microscope
VEGF	vascular endothelial growth factor

## Author details

Matteo Bruno Lodi\* and Alessandro Fanti  
Department of Electrical and Electronic Engineering, University of Cagliari,  
Cagliari, Italy

\*Address all correspondence to: [matteob.lodi@unica.it](mailto:matteob.lodi@unica.it)

## IntechOpen

© 2019 The Author(s). Licensee IntechOpen. This chapter is distributed under the terms of the Creative Commons Attribution License (<http://creativecommons.org/licenses/by/3.0>), which permits unrestricted use, distribution, and reproduction in any medium, provided the original work is properly cited. 

## References

- [1] Liu XL et al. Magnetic nanomaterials for advanced regenerative medicine: The promise and challenges. *Advanced Materials*. 2018;**1804922**:1-13. DOI: 10.1002/adma.201804922
- [2] Adedoyin AA, Ekenseair AK. Biomedical applications of magneto-responsive scaffolds. *Nano Research*. 2018;**11**(10):5049-5064. DOI: 10.1007/s12274-018-2198-2
- [3] Smolkov B et al. A critical review on selected external physical cues and modulation of cell behavior: Magnetic nanoparticles, non-thermal plasma and lasers. *Journal of Functional Biomaterials*. 2019;**10**(1):2. DOI: 10.3390/jfb10010002
- [4] Xia Y et al. Magnetic field and nano-scaffolds with stem cells to enhance bone regeneration. *Biomaterials*. 2018; **183**:151-170. DOI: 10.1016/j.biomaterials.2018.08.040
- [5] Lodi MB. Synthesis and characterization of ferrofluid impregnated magnetic scaffolds for hyperthermia [thesis]. Politecnico di Torino; 2018. Available from: <https://webthesis.biblio.polito.it/8919/1/tesi.pdf>
- [6] Bock N et al. A novel route in bone tissue engineering: Magnetic biomimetic scaffolds. *Acta Biomaterialia*. 2010;**6**(3): 786-796. DOI: 10.1016/j.actbio.2009.09.017
- [7] Banobre-Lopez M et al. Hyperthermia induced in magnetic scaffolds for bone tissue engineering. *IEEE Transactions on Magnetics*. 2014; **50**(11):1-7. DOI: 10.1109/TMAG.2014.2327245
- [8] Tampieri A et al. Intrinsic magnetism and hyperthermia in bioactive Fe-doped hydroxyapatite. *Acta Biomaterialia*. 2012;**8**(2):843-851. DOI: 10.1016/j.actbio.2011.09.032
- [9] Iannotti V et al. Fe-doping-induced magnetism in nano-hydroxyapatites. *Inorganic Chemistry*. 2017;**56**(8): 4446-4458. DOI: 10.1021/acs.inorgchem.6b03143
- [10] Okamoto M. The role of scaffolds in tissue engineering. In: *Handbook of Tissue Engineering Scaffolds*. 1st ed. Vol. 1. Sawston: Woodhead Publishing; 2019. pp. 23-49. DOI: 10.1016/B978-0-08-102563-5.00002-2
- [11] Lanier OL, Monsalve AG, McFetridge PS, Dobson J. Magnetically triggered release of biologics. *International Materials Reviews*. 2019; **64**(2):63-90. DOI: 10.1080/09506608.2018.1446280
- [12] Grief AD, Richardson G. Mathematical modelling of magnetically targeted drug delivery. *Journal of Magnetism and Magnetic Materials*. 2005;**293**(1):455-463. DOI: 10.1016/j.jmmm.2005.02.040
- [13] Fanti A, Lodi MB, Mazzarella G. Enhancement of cell migration rate toward a superparamagnetic scaffold using LF magnetic fields. *IEEE Transactions on Magnetics*. 2016;**52**: 10-18. DOI: 10.1109/TMAG.2016.2583405
- [14] Fanti A, Lodi MB, Vacca G, Mazzarella G. Numerical investigation of bone tumor hyperthermia treatment using magnetic scaffolds. *IEEE Journal of Electromagnetics, RF and Microwaves in Medicine and Biology*. 2018;**2**(4):294-301. DOI: 10.1109/JERM.2018.2866345
- [15] Perez RA et al. Therapeutically relevant aspects in bone repair and regeneration. *Materials Today*. 2015;



18(10):573-589. DOI: 10.1016/j.mattod.2015.06.011

[16] Rosensweig RE. Heating magnetic fluid with alternating magnetic field. *Journal of Magnetism and Magnetic Materials*. 2002;252:370-374. DOI: 10.1016/S0304-8853(02)00706-0

[17] Ng EYK, Kumar SD. Physical mechanism and modeling of heat generation and transfer in magnetic fluid hyperthermia through Néelian and Brownian relaxation: A review. *Biomedical Engineering Online*. 2017;16(36):1-22. DOI: 10.1186/s12938-017-0327-x

[18] Anghileri LJ, Robert J, editors. *Hyperthermia in Cancer Treatment*. 1st ed. Vol. 2. Boca Raton: CRC Press; 2019. 288 p. DOI: 10.1201/9780429266546

[19] Datta NR et al. Local hyperthermia combined with radiotherapy and/or chemotherapy: Recent advances and promises for the future. *Cancer Treatment Reviews*. 2015;41(9):742-753. DOI: 10.1016/j.ctrv.2015.05.009

[20] Landi GT, Arantes FR, Cornejo DR, Bakuzis AF, Andreu I, Natividad E. Ac susceptibility as a tool to probe the dipolar interaction in magnetic nanoparticles. *Journal of Magnetism and Magnetic Materials*. 2017;421:138-151. DOI: 10.1016/j.jmmm.2016.08.011

[21] Hergt R et al. Enhancement of ac-losses of magnetic nanoparticles for heating applications. *Journal of Magnetism and Magnetic Materials*. 2004;280(2):358-368. DOI: 10.1016/j.jmmm.2004.03.034

[22] van Berkum S, Dee JT, Philipse AP, Erne BH. Frequency-dependent magnetic susceptibility of magnetite and cobalt ferrite nanoparticles embedded in paa hydrogel. *International Journal of Molecular Sciences*. 2013;14(5):10162-10177. DOI: 10.3390/ijms140510162

[23] Santini-Araujo E, Kalil RK, Bertoni F, Park Y, editors. *Tumors and Tumor-like Lesions of Bone*. For Surgical Pathologists, Orthopedic Surgeons and Radiologists. London: Springer-Verlag; 2015. 994 p. DOI: 10.1007/978-1-4471-6578-1

[24] Peabody TD, Attar S, editors. *Orthopaedic Oncology*. New York: Springer International Publishing; 2016. 223 p. DOI: 10.1007/978-3-319-07323-1

[25] Lodi MB, Vacca G, Fanti A, Luini L, Vecchi G, Mazzarella G. Numerical comparison of magnetic biomaterials for hyperthermia applications: The osteosarcoma case. In: 2019 13th European Conference on Antennas and Propagation (EuCAP). Krakow, Poland: IEEE; 2019. pp. 1-5. Available from: <http://ieeexplore.ieee.org/stamp/stamp.jsp?tp=&arnumber=8739883&isnumber=8739246>

[26] Bagaria HG, Johnson DT. Transient solution to the bioheat equation and optimization for magnetic fluid hyperthermia treatment. *International Journal of Hyperthermia*. 2005;21(1):57-75. DOI: 10.1080/02656730410001726956

[27] Meikle ST et al. Surface functionalization superparamagnetic nanoparticles conjugated with thermoresponsive poly (epsilon-lysine) dendrons tethered with carboxybetaine for the mild hyperthermia-controlled delivery of VEGF. *Acta Biomaterialia*. 2016;40:235-242. DOI: 10.1016/j.actbio.2016.04.043

[28] Samal SK et al. Multilayered magnetic gelatin membrane scaffolds. *ACS Applied Materials & Interfaces*. 2015;7(41):23098-23109. DOI: 10.1021/acsami.5b06813